

# CHARACTERIZATION OF HIGHLY POROUS 63S BIOACTIVE GLASS SCAFFOLDS FABRICATED BY TWO FOAMING METHODS

SEYED MEHDI MIRHADI\*, #HAMED GHOMI\*\*, RAHMATOLLAH EMADI\*\*\*

\*Department of Materials Engineering, Shahreza Branch, Islamic Azad University, 86145-311, Shahreza, Isfahan, Iran

\*\*Young Researchers and Elite Club, Najafabad Branch, Islamic Azad University, Najafabad, Iran

\*\*\*Biomaterials Group, Department of Materials Engineering, Isfahan University of Technology, Isfahan 84156-83111, Iran

#E-mail: hamed.ghomi@pmt.iaun.ac.ir

Submitted April 16, 2015; accepted June 24, 2015

**Keywords:** Gelcasting, Porosity, Mechanical properties, Bioactive glass, Biomedical applications

*Resorbable 3D macroporous nanostructure 63S bioactive glass scaffolds were fabricated using the two methods of direct foaming of bioactive glass sol and foaming glass slurry for tissue engineering applications. The scaffolds contained an interconnected pore network with macropore sizes in the range of 100 - 400  $\mu\text{m}$ , which provided the potential for tissue ingrowth and vascularization in the human body.*

*The mean values of compressive strength were in the ranges of 0.53 - 0.68 MPa and 0.8 - 0.92 MPa, respectively, for the scaffolds prepared by the first and second methods. The mean values of total and interconnected porosities were in the ranges of 88 - 93 % and 76 - 86 %, respectively. The highly porous and nanosized structure gave rise to a high specific surface area in the scaffolds which stimulated mineralization in the surrounding bones by enhancing bioreactions and leaching of ions from the surface, which facilitate bone repair and fixation. Finally, it was observed that the prepared scaffolds could satisfy the criteria of an ideal scaffold for tissue engineering applications.*

## INTRODUCTION

Scaffolds implanted into a defect site are meant to help *in situ* regeneration of tissues. In tissue engineering applications, scaffolds are seeded with cells and growth factors *in vitro* to produce the basis for a tissue before implantation [1]. This requires scaffolds of appropriate pore size with interconnected pores to promote cell proliferation, vascular ingrowth and nutrient transportation [2].

Certain compositions of bioactive glasses containing  $\text{SiO}_2\text{-CaO-P}_2\text{O}_5$  bond to both soft and hard tissues without forming scar tissue [3-4]. The dissolution products of these bioactive glasses (soluble silicon and calcium) lead to the rapid expression of genes that regulate both osteogenesis and production of growth factors. These characteristics have stimulated extensive investigations into bioactive glass materials used as scaffolds in tissue engineering [1, 3, 5].

Sol-gel derived bioactive glasses, compared to their melt-derived counterparts, reportedly exhibit enhanced resorbability and bioactivity *in vitro* with improved bone bonding *in vivo* [3-7]. This has been attributed to gel glasses exhibiting a mesoporous texture (pores in the range of 2 - 50 nm in diameter), which is inherent to the sol-gel process and increases the specific surface area [1, 3, 8-12].

An ideal scaffold should combine the beneficial properties of bioactive glasses with a structure containing an interconnected network with macropores (greater than 100  $\mu\text{m}$ ) to enable tissue ingrowth [13] and nutrient delivery to the center of the regenerated tissue and mesopores ( $2 \text{ nm} \leq \text{pore size} \leq 50 \text{ nm}$ ) in order to promote cell adhesion [3, 13]. Another requirement is that the scaffold should be resorbed at controlled rates to match that of tissue repair. Furthermore, the processing method used should be capable of producing irregular and complex shapes to match those of the defect in the bone of the patient [1-3, 14]. Foaming sol-gel- derived bioactive glasses, or gelcasting, provides the potential for making scaffolds with these properties [14]. Gelcasting is a well-established method for making high-quality, complex-shaped ceramic pieces by means of *in situ* solidification through which a macromolecular network is created from the *in situ* polymerization of an organic gelling agent [15-17].

The objective of the present work was to fabricate and characterize bioactive glass scaffolds with interconnected pores of diameters in excess of 100  $\mu\text{m}$  using the foaming process. For this purpose, different scaffolds were produced by both direct foaming of bioactive glass sol and foaming glass slurry. Finally, the morphology and mechanical properties of the two types of scaffolds thus prepared were compared to ensure the achievement of the desired properties.

## EXPERIMENTAL

### Starting materials

In this study, calcium nitrate tetrahydrate ( $\text{Ca}(\text{NO}_3)_2 \cdot 4\text{H}_2\text{O}$ , Merck), triethyl phosphate (TEP, Aldrich), tetraethyl orthosilicate (TEOS, Merck), hydrochloric acid (HCl, Merck), and absolute ethanol ( $\text{C}_2\text{H}_5\text{OH}$ , Merck) were used as bioactive glass (BG) precursors. The gelling components used included hydrofluoric acid (HF, Merck) and agarose powder (Merck) as the gelling agents, Tergitol (Aldrich) as a surfactant, and tripolyphosphate sodium (TPP) as a dispersant. The gelling agent used for the direct foaming of bioactive glass sol was hydrofluoric acid and that for foaming glass slurry was agarose powder.

### Preparation of scaffolds by foaming glass slurry

Following the procedures reported elsewhere [18], 63S BG powder with 65 %  $\text{SiO}_2$ , 31 %  $\text{CaO}$ , and 4 %  $\text{P}_2\text{O}_5$  in molar percentages were prepared. Briefly, TEOS was dissolved in absolute ethanol and deionized water, using 2 M HCl as the catalyst, and stirred for 30 min. The TEP was then dissolved into the prepared solution, to which  $\text{Ca}(\text{NO}_3)_2 \cdot 4\text{H}_2\text{O}$  was added after 20 min. The clear solution was then aged at  $60^\circ\text{C}$  for 48 h and dried at  $120^\circ\text{C}$  for 48 h. The powder thus obtained was calcined at  $600^\circ\text{C}$  for 2 h, which was then dispersed in double distilled water by using 1 wt. % TPP as the dispersant. Agarose powder (7 wt. %) was simultaneously dissolved as the gelling agent in double distilled water by heating up to  $130^\circ\text{C}$ . The two solutions were then mixed at  $80^\circ\text{C}$  to obtain a slurry which was then foamed by adding 3 volume percent (vol. %) of Tergitol while vigorously agitated using a triple-blade mixer before it was poured into the mold. The gelling reaction was conducted by cooling the samples to  $0^\circ\text{C}$ . The samples were then demolded, dried at ambient temperature, and sintered at 800 and  $900^\circ\text{C}$  for 4 h.

### Preparation of scaffolds by direct foaming of bioactive glass sol

The glass sol was prepared as described above. Before aging and drying, simultaneous hydrolysis and polycondensation reactions were allowed to occur during and after sol preparation. Briefly, aliquots of 30 ml of the sol were foamed by vigorous agitation while 1 ml of the surfactant (Tergitol), double distilled water, and 3 ml of hydrofluoric acid (HF, a catalyst for polycondensation) were added. As viscosity increased rapidly and the gelling point was approached, the solution was poured into molds. The gelation process provided permanent stabilization for the bubbles that formed by air entrapment during the early stages of foaming as the result of reduced surface tension and vigorous agitation

of the solution. The scaffolds were then aged at  $60^\circ\text{C}$  for 48 h, dried at  $120^\circ\text{C}$  for 48 h, and sintered at 800 and  $900^\circ\text{C}$  for 4 h.

### Materials characterization

#### X-ray diffraction analysis

Phase structure analysis of the powder and the scaffolds thus prepared was performed using an X-ray diffractometer (XRD, Philips Xpert) with Ni filtered  $\text{Cu } \alpha$  ( $\lambda_{\text{Cu } \alpha} = 0.154186 \text{ nm}$ , radiation at 30 mA, and 40 kV) in the range of  $20 \leq 2\theta \leq 70$  (time per step: 1 s and step size:  $0.05^\circ$ ).

#### Specific surface area

The specific surface area of the prepared BG powder was determined by physical adsorption of nitrogen gas at  $-196^\circ\text{C}$  on the surface of the powder and by calculating the amount of adsorbate gas corresponding to a monomolecular layer on the surface (Micromeritics Instrument Corp., Gemini). Assuming a hexagonal close packing, the adsorptive gas ( $\text{N}_2$ ) has a molecular cross sectional area of  $0.162 \text{ nm}^2$  at  $-196^\circ\text{C}$  [19].

The specific surface area of the powder was estimated using the multipoint Brunauer-Emmett-Teller (BET) adsorption isotherm equation in its linear form:

$$\left[ \frac{P}{V_a(P_o - P)} \right] = \frac{C-1}{V_m C} \times \frac{P}{P_o} + \frac{1}{V_m C} \quad (1)$$

where,  $P$  and  $P_o$  are the equilibrium and saturation pressures of the adsorbates at  $-196^\circ\text{C}$ ,  $V_a$  is the volume of gas adsorbed at standard temperature and pressure (STP),  $V_m$  is the volume of the monolayer adsorbed gas, and  $C$  is the BET constant that is related to the enthalpy of adsorption of the adsorbate gas on the powder.

The BET value  $[P/(V_a(P_o - P))]$  was plotted against  $P/P_o$  according to Equation 1 (i.e., the BET plot). This plot should yield a straight line usually in the approximate relative pressure range of 0.05 to 0.3. The value of the slope and the y-intercept of the line were used to calculate  $V_m$  and  $C$ . The following equations were used:

$$V_m = \frac{1}{(\text{slope} + \text{intercept})} \quad (2)$$

$$C = \frac{\text{slope}}{\text{intercept}} + 1 \quad (3)$$

The specific surface area,  $S_{\text{BET}}$ , in  $\text{m}^2 \cdot \text{g}^{-1}$ , was calculated using Equation 4 [20]:

$$S_{\text{BET}} = \frac{V_m \times N \times A}{22\,400} \quad (4)$$

Average particle size of the prepared powder was calculated using Equation 5 based on the assumption that the synthesized particles were spheroids:

$$d = \frac{6 \times 10^3}{2.87 \times S_{BET}} \quad (5)$$

where,  $d$  is the average particle size (nm),  $S_{BET}$  is the specific surface area ( $\text{m}^2 \cdot \text{g}^{-1}$ ), and 2.87 is the theoretical density of 63S BG.

#### Scanning electron microscopy analysis

Scanning electron microscopy (SEM, Philips XL 30) was used to study the morphology and size of the pores in the BG scaffolds. Pore size distribution was determined based on the results of image analysis of SEM micrographs. The scaffolds were sputter-coated with a thin layer of gold (about several nanometers thick) using a physical vapor deposition apparatus for improved resolution.

#### Transmission electron microscopy analysis

Transmission electron microscopy (TEM, Philips CM-200) was used to study the particle size of the BG powders.

#### Porosity measurement

The porosity of the scaffolds which may be either interconnected or closed was measured according to the Archimedes method [21]. Apparent porosity or interconnected porosity was determined using Equation 6:

$$\text{Apparent porosity} = [(W_w - W_d)/(W_w - W_s)] \times 100 \quad (6)$$

where,  $W_d$  is the weight of the dry scaffold,  $W_s$  is the weight of the scaffold suspended in water, and  $W_w$  is the weight of the scaffold after it is removed from water.

True porosity expressed by Equation 7 includes both interconnected and closed pores of the scaffold:

$$\text{True porosity} = [(\rho(W_w - W_s) - W_d)/(\rho(W_w - W_s))] \times 100 \quad (7)$$

where,  $\rho$  is the true density or specific gravity of the glass.

In order to check the validity of the results obtained, the diameter and the height of the scaffolds were measured using a digital caliper rule and the mass of the samples was measured using a digital balance. The value of green density ( $\rho_g$ ) was determined as shown in Equation 8:

$$\rho_g = W_d/(\pi r^2 h) \quad (8)$$

where,  $r$  is the radius (cm) and  $h$  is the height (cm) of the sample. The percentage of porosity was measured with respect to density, as shown in Equation 9:

$$\text{True porosity} = [1 - (\rho_g/2.87)] \times 100 \quad (9)$$

where, 2.87 is the theoretical density of BG.

#### Mechanical testing

The compression test has been widely used for characterizing the mechanical properties of porous scaffolds. In this study, parallel plate compression tests were carried out on cylindrical scaffolds (20 mm in height and 10 mm in diameter) using a universal testing machine (Zwick, material prufung, 1,446-60) with a crosshead speed of  $0.5 \text{ mm} \cdot \text{min}^{-1}$ . Five samples were used for each sintering temperature and fabrication method and the results were reported as average values. Compressive strength was evaluated from the maximum point of the stress/strain graph, which occurs when the first crack appears on the scaffold. Elastic modulus was calculated as the slope of the initial linear portion of the stress/strain graph.

## RESULTS AND DISCUSSION

Figure 1a shows the adsorption isotherm of nitrogen at  $-196^\circ\text{C}$  on the BG powder and Figure 1b shows the related BET plot. The values of BET specific surface area and  $C$  calculated from the linear part of the BET plot were determined to be  $189.7 \text{ m}^2 \cdot \text{g}^{-1}$  and 57.8, respectively. Assuming powder particles to be spherical, the average particle size calculated using Equation 5 was found to be 11 nm. The high specific surface area can be attributed to both the sol-gel preparation method and the nano-sized particles, which leads to excellent bioactivity, osteoconductivity, and biodegradability providing fast bone ingrowth and improved bone bonding *in vivo* [3-7, 14]. The values of particle size obtained from the results of image analysis of TEM micrographs also confirmed the above results. The TEM micrograph of the BG nanopowder (Figure 2) indicates a particle size of less than 30 nm.

The XRD patterns of the BG nanopowder and the scaffolds prepared by foaming glass slurry at different sintering temperatures are shown in Figure 3. Clearly, the observed pattern of BG nanopowder (Figure 3a) confirms the formation of BG with an amorphous structure. In addition, no peak of diffraction is observed in the spectrum of the BG scaffold sintered at  $800^\circ\text{C}$  (Figure 3b), indicating that the scaffold cannot have a crystalline structure and that it, therefore, has a glass structure. However, the spectrum of the BG scaffold sintered at  $900^\circ\text{C}$  (Figure 3c) exhibits peaks indicative of Larnite ( $\text{Ca}_2\text{SiO}_4$ ) [22]. It should be noted that the crystallinity of BG increased upon heat treatment at  $900^\circ\text{C}$ . This is due to the formation of the crystalline phase (Larnite) at approximately  $900^\circ\text{C}$ , which affected the resorbability and bioactivity of the amorphous BG [23]. The XRD patterns of the scaffolds prepared by direct foaming of bioactive glass sol at different sintering temperatures are shown in Figure 4. In agreement with the above results, the scaffold sintered at  $800^\circ\text{C}$  exhibits an amorphous structure but the one sintered at  $900^\circ\text{C}$  exhibits partial crystallization of BG to the Larnite ( $\text{Ca}_2\text{SiO}_4$ ) phase.

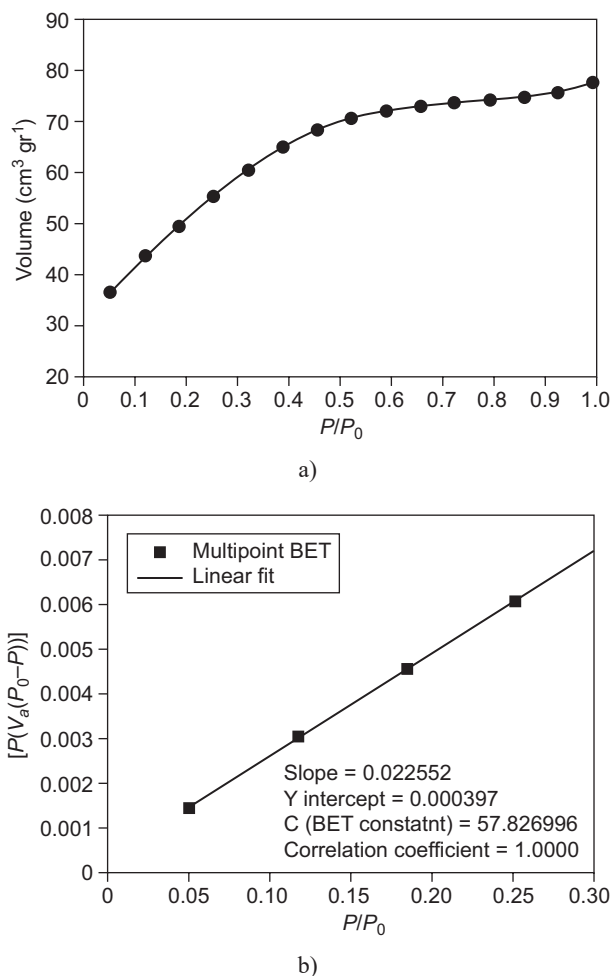


Figure 1. Adsorption isotherm of nitrogen at -196°C (b) BET plot for nitrogen adsorbed at -196°C on the BG powder prepared.

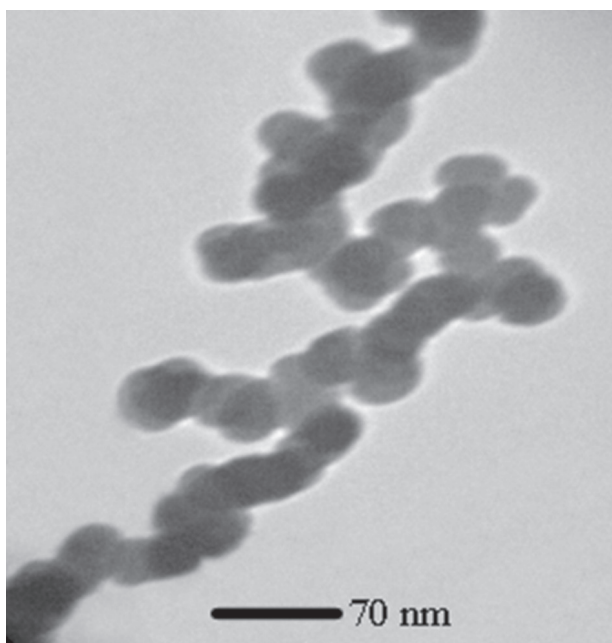


Figure 2. TEM micrograph of the prepared BG nanopowders.

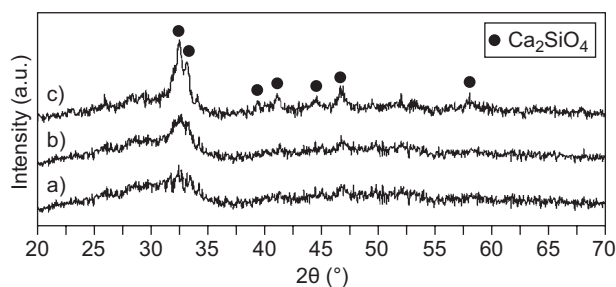


Figure 3. XRD patterns of the a) BG nanopowder, and b), c) scaffolds prepared by foaming glass slurry sintered at 800° and 900°C for 4 hour, respectively.

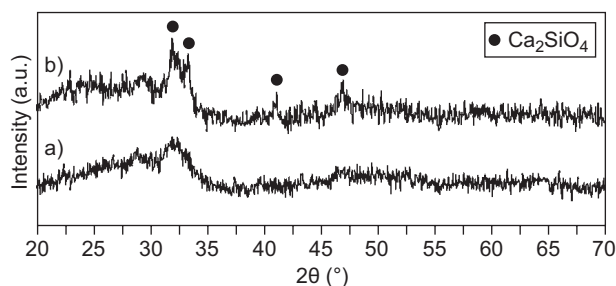


Figure 4. XRD patterns of the scaffolds prepared by direct foaming of bioactive glass sol sintered at a) 800°C and b) 900°C for 4 hr.

The mean values of compressive strength and the elastic modulus of the scaffolds prepared by foaming glass slurry at different sintering temperatures measured in the ranges of 0.8 - 0.92 MPa and 50 - 57 MPa, respectively. The values recorded for the same parameters in the case of the scaffolds prepared by direct foaming of bioactive glass sol at different sintering temperatures were in the ranges of 0.53 - 0.68 MPa and 49 - 59 MPa (Table 1). Total porosity in the scaffolds prepared by foaming glass slurry and sintered at different temperatures ranged from 88 to 90 %, while open porosity in the same scaffolds ranged from 76 to 80 %. On the other hand, the total porosity and open porosity values recorded for the scaffolds fabricated by direct foaming of bioactive glass sol at different sintering temperatures ranged over 90 - 93 and 81 - 86 %, respectively (Table 1).

The differences observed in the mechanical properties of the two types of scaffolds were attributed to differences in porosity, pore size, pore structure, and pore morphology. In other words, the scaffolds prepared by direct foaming of bioactive glass sol exhibited higher porosity, interconnectivity, and pore size distribution. Sintering at 800°C for 4 h provides an optimal combination of amorphous structure and compressive strength together with macroscopic structural features favorable to bone ingrowth and angiogenesis [13]. This is while, due to the bioactivity of the Larnite phase, the scaffolds sintered at 900°C are appropriate for applications in which higher strengths are needed to withstand greater loadings. Table 1 shows the porosity and mechanical

properties of the scaffolds as a function of the preparation method employed and the sintering temperature applied. The increase in mechanical properties with sintering may be attributed to the densification of the struts and the reduced porosity of the foams.

The mechanical properties of bioceramic scaffolds highly depend on their composition, porosity, pore size, and pore geometry. Increased porosity and pore size lead to significant reductions in mechanical properties. In addition, the shapes and dimensions of the samples used affect the measured values of mechanical properties. Clearly, compressive strength decreases with increasing surface area of the test sample. This is because the material volume is proportional to the end surface area; the higher the volume, the higher the density of the defects contained in the scaffold.

Comparisons of the mechanical and physical properties of different scaffolds including those prepared in this study are presented in Table 2. Obviously, better values of compressive strength were obtained for bioceramic scaffolds fabricated in this study than those for

similar scaffolds reported in the literature. Chen et al. [24-26] reported far lower values of compressive strength for their highly porous (~ 90 %) Bioglass® scaffolds. Foams obtained by the replication method exhibit hollow centers in the struts that would lead to degraded mechanical properties, which is in contrast to the scaffolds fabricated in the present study which show more uniform and denser walls. The compressive strength of spongy bones (not the strut) is in the range of 0.2 - 4 MPa while their relative density is about 0.1 [26]. The compressive strength (0.53 - 0.92 MPa) measured in the scaffolds prepared in this study falls within this range, which is sufficient for such conditions as manipulation during SBF tests. In addition, the compressive strength of hydroxyapatite scaffold has been reported to increase significantly *in vivo* due to tissue ingrowth. There is, therefore, no need for fabricating scaffolds with mechanical strengths similar to those of the bone since the cells growing on the scaffold and the new tissue forming *in vitro* will make a biocomposite that enhances the strength of the scaffold to the levels required [29].

Table 1. Porosity and mechanical properties of the scaffolds as a function of the preparation method employed and the sintering temperature applied.

Preparation method	Sintering temperature	True porosity (%) (S.D.)*	Apparent porosity (%) (S.D.)	Compressive strength (MPa) (S.D.)	Elastic modulus (MPa) (S.D.)
Foaming glass slurry	800°C	90 (± 1)	80 (± 2)	0.8 (± 0.07)	50 (± 5)
Foaming glass slurry	900°C	88 (± 2)	76 (± 2)	0.92 (± 0.09)	57 (± 11)
Direct foaming of bioactive glass sol	800°C	93 (± 1.5)	86 (± 2)	0.53 (± 0.12)	49 (± 9)
Direct foaming of bioactive glass sol	900°C	90 (± 2)	81 (± 1)	0.68 (± 0.05)	59 (± 7)

\* Standard deviation

Table 2. Overview of the mechanical and physical properties for various scaffolds prepared by different procedures including the one employed this study.

Material	Process	Compressive strength (MPa)	Pore sizes (µm)	Porosity (%)	Compression test samples	Ref.
70S30C	Foaming sol-gel derived bioactive glasses	1.6-2.5	200-600	81-90	Cylindrical foams (D=27 mm; L=9 mm)	5
70S30C	Foaming sol-gel derived bioactive glasses	0.34-2.26	–	82-88	Cylindrical foams (D=27 mm; L=9 mm)	8
45S5 BG	Replication technique	0.1-0.15	-	92-94	Rectangular in shape: 10 mm in height and 3×3 mm in cross-section	24
45S5 BG	Replication/slurry-dipcoating technique	0.42	–	90	–	25
45S5 BG	Replication technique	0.27-0.42	510-720	89-92	Rectangular in shape: 10 mm in height and 5×5 mm in cross-section	26
45S5 BG	Mix with an aqueous solution, compressed, then calcined	5.4-7.2	420 in length 100 in breadth	5.4-7.2	–	27
45S5 BG	Powder metallurgy-polymer foam technologies	1.7-5.5	335-530	64-79	Cylindrical foams (D=9-12 mm; L=3-8 mm)	28
63S BG	Foaming glass slurry	0.8-0.92	100-400	88-90	Cylindrical scaffolds (D=10 mm; L=20 mm)	This study
63S BG	Direct foaming of bioactive glass sol	0.53-0.68	100-400	90-93	Cylindrical scaffolds (D=10 mm; L=20 mm)	This study

The morphology, size distribution, and pore interconnectivity of the scaffolds fabricated by both methods in this study and sintered at 900°C for 4 h are shown in the SEM micrographs presented in Figure 5.

Based on these micrographs, the scaffold structure contains a highly interconnected spherical porous network with a pore size ranging between 100 and 400 μm. It is also seen that, in addition to the macropores which provide the potential for tissue ingrowth, the scaffolds exhibit a large amount of micropores which

enhance both the release of ionic products and bioactivity. Interconnected pores are highly important as they allow for body fluid circulation and replacement, nutritional supply, ion diffusion, osteoblast cell penetration, and vascularization [8, 14, 30-31]. Pores with interconnected diameters of less than 100 μm do not allow for efficient *in vivo* tissue ingrowth and vascularization so that the damaged tissue will not be fully restored [3, 32]. Changes in macroporosity and textural porosity of the scaffolds due to changes in the fabrication process may

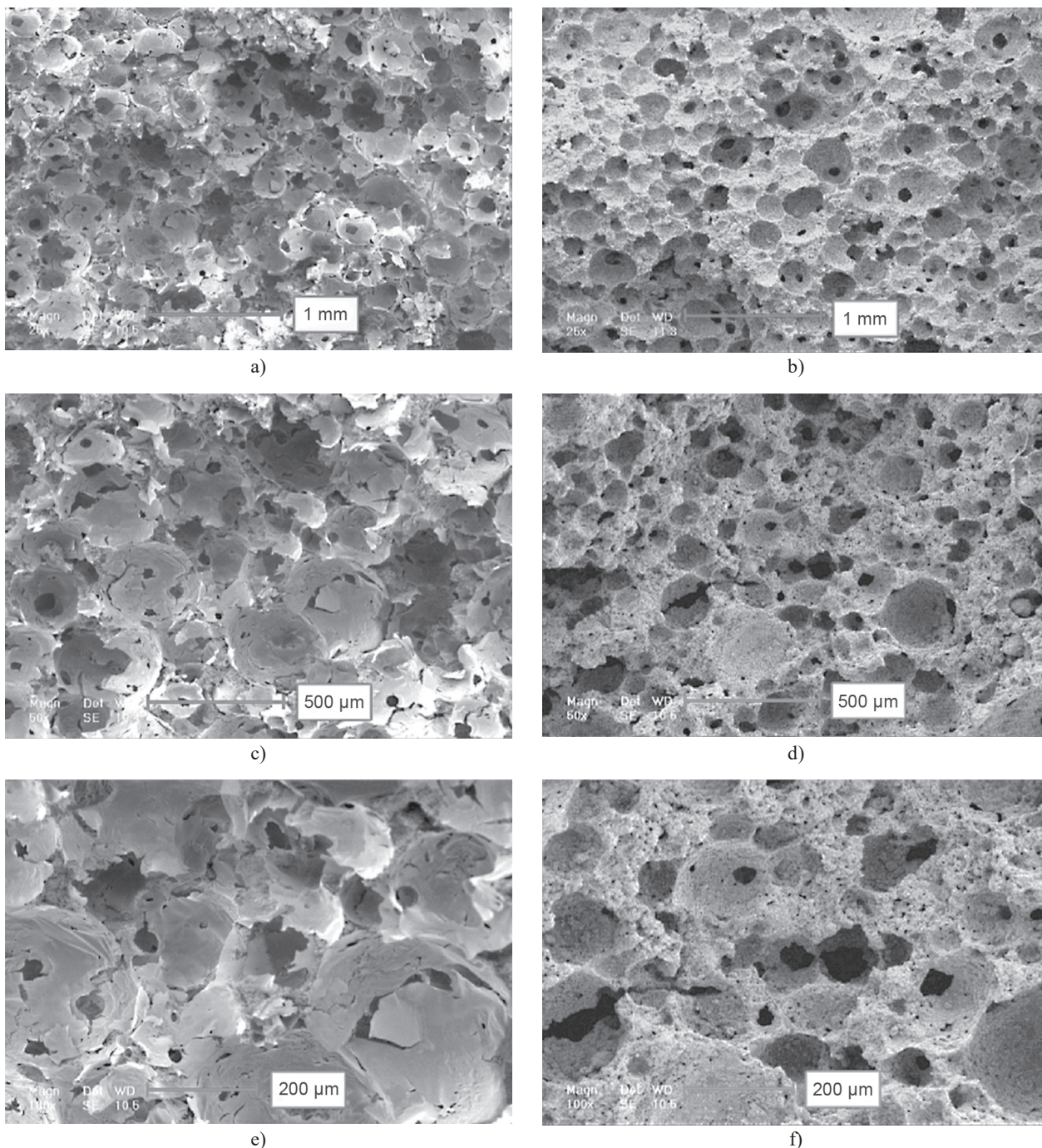


Figure 5. SEM micrographs of the scaffolds prepared by: a, c, e) foaming glass slurry, and b, d, f) direct foaming of bioactive glass sol sintered at 900°C for 4 h at different magnifications.

lead to changes in the dissolution rate and, thereby, the bioactivity of the scaffold. Moreover, changes in the glass dissolution rate would affect the number of ionic products released by the glass, products that act as genetic stimuli. An important factor in supplying the ion dosage required for genetic stimulation is the ability to control the dissolution rate of a scaffold to match that of tissue regeneration [32].

Bioactive glasses have been of great interest due to their excellent osteoconductivity, bioactivity, biocompatibility, ability to deliver cells [26], and controllable biodegradability, which make them promising scaffold materials for tissue engineering applications [29, 33].

Porous bioceramics have been used for bone repair and reconstruction to promote the regeneration of damaged tissues as a template for cell interaction and new tissue ingrowth. In fact, porous bioceramics have been used for implant fixation via bone ingrowth (i.e., biological fixation), bone defect filling, bone regeneration via tissue engineering, cell loading, drug delivery, and ocular implant [14, 30-31]. Over the past few decades, important research efforts have been directed at developing porous scaffolds with optimized structure, properties, and composition.

An ideal bone tissue scaffold should contain an interconnected porous structure; that is, it should be highly permeable with a porosity > 90 % and a pore size in the range of 10-500  $\mu\text{m}$  which make it not only suitable for cell seeding, tissue ingrowth, and vascularization but also for nutrient delivery and waste removal [34]. Furthermore, it should have desirable mechanical strength, biocompatibility, osteoconductivity, and biodegradability [8, 14].

The manufacturing method employed in this study is a well-established one for making ceramics green body with short forming time, high yields, high green strength, and low-cost machining. It has, indeed, been used for preparing high-quality and complex-shaped dense/porous ceramic parts [15]. The scaffolds manufactured by the foaming process in this study have a spherical interconnected pore network with sufficient pore size and compressive strength that could be a promising candidate for use in tissue engineering.

## CONCLUSIONS

Two foaming methods were used to fabricate nanostructure 63S bioactive glass scaffolds with 65 %  $\text{SiO}_2$ , 31 %  $\text{CaO}$ , and 4 %  $\text{P}_2\text{O}_5$  (in mol. %). The scaffolds prepared by direct foaming of bioactive glass sol and foaming glass slurry exhibited compressive strengths of 0.53 - 0.68 MPa and 0.8 - 0.92 MPa, respectively. The scaffolds showed an interconnected pore network with macropores (100 - 400  $\mu\text{m}$ ), a total porosity in the range of 88 - 93 %, and an interconnected porosity in the range of 76 - 86. These properties make it possible to use

these scaffolds in tissue ingrowth and vascularization in the human body. Due to their nanosized structure and high porosity, the scaffolds have a high specific surface area that enhances their bioreactions and ionic leaching from the surface that stimulate mineralization of the surrounding bones, thereby facilitating bone repair and fixation. The combination of these properties and those intrinsic to the sol-gel derived bioactive glass (such as bone bonding, osteoproduction, and bioresorbability) as well as the dissolution products stimulate osteogenesis at the genetic level. Hence, these scaffolds may be claimed to be capable of meeting the stringent criteria for an ideal scaffold and to have a high potential for use in bone tissue engineering applications.

## Acknowledgement

*The authors are grateful for support of this research by Isfahan University of Technology.*

## REFERENCES

1. Jones J.R., Hench L.L.: *Journal of Materials Science* 38, 3783 (2003).
2. Gao C., Deng Y., Feng P., Mao Z., Li P., Yang B., Deng J., Cao Y., Shuai C., Peng S.: *International Journal of Molecular Sciences* 15, 4714 (2014).
3. Jones J.R., Hench L.L.: *Journal of Biomedical Materials Research Part B: Applied Biomaterials* 68, 36 (2004).
4. Zhong J., Greenspan D.C.: *Journal of Biomedical Materials Research Part B: Applied Biomaterials* 53, 694 (2000).
5. Jones J.R., Ehrenfried L.M., Saravanapavan P., Hench L.L.: *Journal of Materials Science: Materials in Medicine* 17, 989 (2006).
6. Hamadouche M., Meunier A., Greenspan D.C., Blanchat C., Zhong J.P., Torre G.P.L., Sedel L.: *Journal of Biomedical Materials Research* 54, 560 (2001).
7. Arcos D., Greenspan D.C., Vallet-Regi M.: *Journal of Biomedical Materials Research A* 65, 344 (2003).
8. Jones J.R., Ehrenfried L.M., Hench L.L.: *Biomaterials* 27, 964 (2006).
9. Sepulveda P., Jones J.R., Hench L.L.: *Journal of Biomedical Materials Research* 61, 301 (2002).
10. Li R., Clark A.E., Hench L.L.: *Chemical Processing of Advanced Materials* 56, 627 (1992).
11. Pereira M.M., Clark A.E., Hench L.L.: *Journal of the American Ceramic Society* 78, 2463 (1995).
12. FitzGerald V., Martin R.A., Jones J.R., Qiu D., Wetherall K.M., Moss R.M., Newport R.J.: *Journal of Biomedical Materials Research Part A* 91, 76 (2009).
13. Freyman T.M., Yannas I.V., Gibson L.J.: *Progress in Materials Science* 46, 273 (2001).
14. Shirliff V.J., Hench L.L.: *Journal of Materials Science* 38, 4697 (2003).
15. Yang J., Yu J., Huang Y.: *Journal of the European Ceramic Society* 31, 2569 (2011).
16. Ghomi H., Fathi M.H., Edris H.: *Ceramics International* 37, 1819 (2011).

17. Ghomi H., Fathi M.H., Edris H.: *Journal of Sol-Gel Science and Technology* 58, 642 (2011).
  18. Ghomi H., Fathi M.H., Edris H.: *Materials Research Bulletin* 47, 3523 (2012).
  19. Sing K.S.W., Everett D.H., Haul R.A.W., Moscou L., Rouquerol R.A., Rouquerol J., Siemiewska T.: *Pure and Applied Chemistry* 57, 603 (1985).
  20. Will J., Melcher R., Treul C., Travitzky N., Kneser U., Polykandriotis E., Horch R., Greil P.: *Journal of Materials Science: Materials in Medicine* 19, 2781 (2008).
  21. Askeland D.R.: *The Science and Engineering of Materials*. 2nd ed., PWS Pub. Co. 1989.
  22. XRD JCPDS data file No. 00-020-0237.
  23. Atwood R.C., Jones J.R., Lee P.D., Hench L.L.: *Scripta Materialia* 51, 1029 (2004).
  24. Chen Q.Z., Efthymiou A., Salih V., Boccaccini A.R.: *Journal of Biomedical Materials Research Part A* 84, 1049 (2008).
  25. Chen Q.Z., Mohn D., Stark W.J.: *Journal of the American Ceramic Society* 94, 4184 (2011).
  26. Chen Q.Z., Thompson I.D., Boccaccini A.R.: *Biomaterials* 27, 2414 (2006).
  27. Wu S.C., Hsu H.C., Hsiao S.H., Ho W.F.: *Journal of Materials Science: Materials in Medicine* 20, 1229 (2009).
  28. Aguilar-Reyes E.A., Leon-Patino C.A., Jacinto-Diaz B., Lefebvre L.P.: *Journal of the American Ceramic Society* 95, 3776 (2012).
  29. Jones J.R., Hench L.L.: *Current Opinion in Solid State and Materials Science* 7, 301,(2003).
  30. Oh S., Oh N., Appleford M., Ong J.L.: *American Journal of Biochemistry and Biotechnology* 2, 49 (2006).
  31. Jones J.R., Lee P.D., Hench L.L.: *Philosophical Transactions of the Royal Society A: Mathematical Physical and Engineering Science* 364, 263 (2006).
  32. Jones J.R., Hench L.L.: *Journal of Materials Science and Technology* 17, 891 (2001).
  33. Boccaccini A.R.: *Journal of Materials Science: Materials in Medicine* 14, 350 (2003).
  34. Gerhardt L.C., Boccaccini A.R.: *Materials* 3, 3867 (2010).
-